Masses classification using fuzzy active contours and fuzzy decision trees

G. J. Palma[a,b], G. Peters[c*], S. Muller[a], I. Bloch[b]

[a] GE Healthcare Europe, 283, rue de la Minière, 78530 Buc, France
[b] Ecole Nationale Supérieure des Télécommunications (GET-Télécom Paris)
CNRS UMR 5141, 46, rue Barrault, 75013 Paris, France
[c] Fenics, Le Gemellyon Sud, 59, bvd Vivier Merle, 69429 Lyon Cedex 03

ABSTRACT

In this paper we propose a method to classify masses in digital breast tomosynthesis (DBT) datasets. First, markers of potential lesions are extracted and matched over the different projections. Then two level-set models are applied on each finding corresponding to spiculated and circumscribed mass assumptions respectively. The formulation of the active contours within this framework leads to several candidate contours for each finding. In addition, a membership value to the class *contour* is derived from the energy of the segmentation model, and allows associating several fuzzy contours from different projections to each set of markers corresponding to a lesion. Fuzzy attributes are computed for each fuzzy contour. Then the attributes corresponding to fuzzy contours associated to each set of markers are aggregated. Finally, these cumulated fuzzy attributes are processed by two distinct fuzzy decision trees in order to validate/invalidate the spiculated or circumscribed mass assumptions.

The classification has been validated on a database of 23 real lesions using the leave-one-out method. An error classification rate of 9% was obtained with these data, which confirms the interest of the proposed approach.

Keywords: CAD, Digital Breast Tomosynthesis, fuzzy active contours, fuzzy decision trees

1. INTRODUCTION

Digital Breast Tomosynthesis (DBT) is a new 3D imaging technique. The 3D reconstruction of the breast from a set of low-dose projections intends to overcome the superimposition of tissues in the breast that leads to obscured lesions and false alarms. The accurate detection and localization of mass lesions, which may be a sign of breast cancer in 2D mammograms, remains an important diagnosis step. Computer Aided Detection (CAD) has the potential to increase the detection sensitivity of radiologists. With the expected increased volume of data to read in DBT exams, the availability of a CAD system is becoming increasingly important. Furthermore, circumscribed and spiculated masses are typical of benign and malignant lesions respectively. It becomes therefore critical to develop an efficient algorithm for this classification task. We introduce a new segmentation and classification approach based on fuzzy active contours and fuzzy decision trees that is a suitable alternative to conventional approaches[1] for this purpose.

2. GLOBAL SCHEME

Our approach is based on the detection and segmentation of structures directly on the projections, which may be faster than processing a reconstructed volume when few acquisitions are acquired and has the advantage of being reconstruction independent. Then we associate the result of the segmentation in the different projected views, extract some features and aggregate the results in order to make a decision.[2] This last step is done two times using different assumptions about the findings (circumscribed or spiculated). The goal of this decision step will be to validate or invalidate these assumptions.

*G. Peters was GE Healthcare employee and ENST PhD student during the development of the work presented in this paper. Send correspondence to giovanni.palma@ge.com.

Medical Imaging 2008: Computer-Aided Diagnosis, edited by Maryellen L. Giger, Nico Karssemeijer
Proc. of SPIE Vol. 6915, 691509, (2008) · 1605-7422/08/$18 · doi: 10.1117/12.770078

2.1 Makers

First, some markers need to be placed on the projected masses. While this can be achieved using several approaches, for instance using the result of the convolution of the projection images with wavelets,[3] in our study an expert manually marked the lesions. In this paper, we only address the classification of a finding as *spiculated* or *circumscribed*.

2.2 Multiple hypotheses

In order to describe the type of a lesion, we consider two hypotheses (see Figure 1) for each finding: either it is a spiculated mass, or a circumscribed one. This results in two kinds of a priori on the shape of mass contours. These two hypotheses will be translated into a priori information in the segmentation process. The key point discussed in this article will be to validate or invalidate these hypotheses.

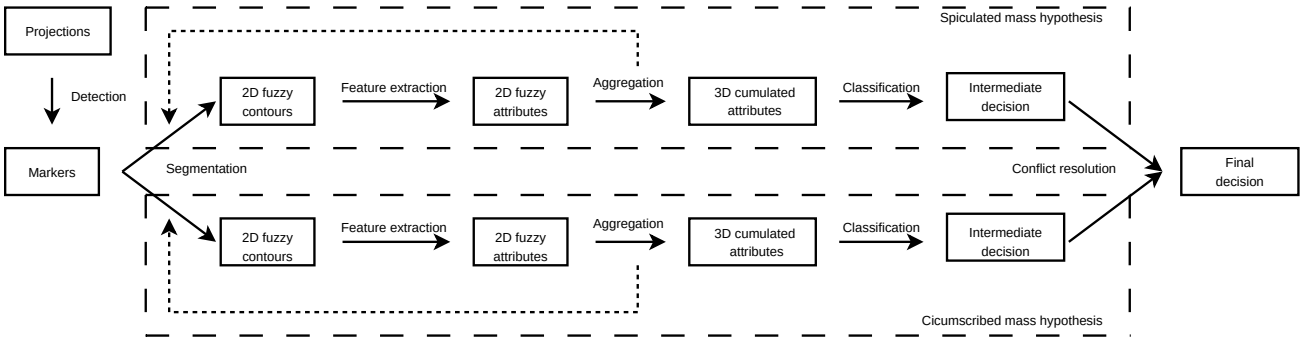

Figure 1. Global scheme of the algorithm.

To achieve this goal each finding will be segmented into two sets of contours using two sets of parameters corresponding to each hypothesis. This is done using fuzzy active contours as detailed in Section 3. Then, for each model, the results of each segmentation along the projections for the same finding are aggregated and classified using fuzzy decision trees as shown in Section 4.

3. FUZZY CONTOURS EXTRACTION

We now propose a way to segment the findings in the projections. Since a unique contour for a given finding is sometimes difficult to define, our segmentation approach relies on the extraction of a set of contours. A membership degree is associated to each contour, which enables us to use fuzzy set theory, which is suitable not only to handle imprecision of the lesion, but also for the aggregation of information collected amongst the projections.

3.1 Segmentation using fuzzy active contours

We use the level-set framework to express and solve this particular finding segmentation problem. This mainly relies on the representation of the contours by a Lipschitz continuous function[4,5] $\phi : \Omega \rightarrow \mathbb{R}$. This function is interpreted as follows:

$$\forall p \in \Omega \quad \begin{cases} \phi(p) > 0 & \textit{if } p \textit{ is inside the contour} \\ \phi(p) = 0 & \textit{if } p \textit{ is on the contour} \\ \phi(p) < 0 & \textit{if } p \textit{ is outside the contour} \end{cases} \tag{1}$$

with p a point of the image domain Ω.

Now, using this framework, the problem is modeled using an energy previously introduced[6] with two sets of parameters corresponding to each hypothesis. This energy is a hybrid model that takes into account the regularity, the gradient under the contours and the homogeneity of the segmented regions:

$$E(\phi) = \mu \int_{\Omega} \delta(\phi(p))|\nabla\phi(p)|dp + \nu \int_{\Omega} H(\phi(p))dp + \alpha E_{region}(\phi) + \beta E_{edge}(\phi) + \gamma E_{pressure}(\phi) \tag{2}$$

with H the Heavyside function, δ its derivative (the Dirac distribution) and:

$$E_{region}(\phi) = \lambda_1 \int_\Omega |I(p) - \overline{c_1}|^2 H(\phi(p))dp + \lambda_2 \int_\Omega |I(p) - \overline{c_2}|^2 (1 - H(\phi(p)))dp \quad (3)$$

with I the image to segment, $\overline{c_1}$ and $\overline{c_2}$ the mean gray values inside and outside the contour.

$$E_{edge}(\phi) = -\int_\Omega \delta(\phi(p)) g(|I(p)|)dp \quad (4)$$

where $g(|I(p)|)$ is a stopping function designed to slow down the contour in the vicinity of the edges, and is given by:

$$g(|I(p)|) = |\nabla(G(p) * I(p))|$$

where $G * I$, a smoother version of I, is the convolution of the image I with the Gaussian G. The function $g(|I(x,y)|)$ is zero in homogenous regions and large at the edges.

Finally, the pressure term is given by:

$$E_{pressure}(\phi) = \int_\Omega \delta(\phi(p))dp \quad (5)$$

According to the hypothesis made, different sets of parameters μ, ν, α, β, γ, λ_1 and λ_2 are used, letting us to introduce the corresponding a priori (e.g. a higher value of μ will be used for circumscribed masses since they are more regular than spiculated masses). To actually resolve such a problem, an evolution scheme is derived from the energy.[5,7,8] This evolution scheme is expressed as the derivative of the energy according to the time.

3.2 From a Lipschitz function to a fuzzy contour

Using an evolution scheme similar to the one proposed for active contours without edges,[7] we can observe that the level 0 is not the only suitable contour candidate. Actually, this evolution scheme is interesting since the Dirac distribution and the Heavyside function are approximated by functions that have non negligible values almost everywhere in the image. This results in a $\frac{\partial \phi}{t}$ that makes the function ϕ evolve not only near the contour but also farther away. Thus, our approach consists to slice the resulting function after convergence in order to get a set of several candidate contours (see Figure 2).

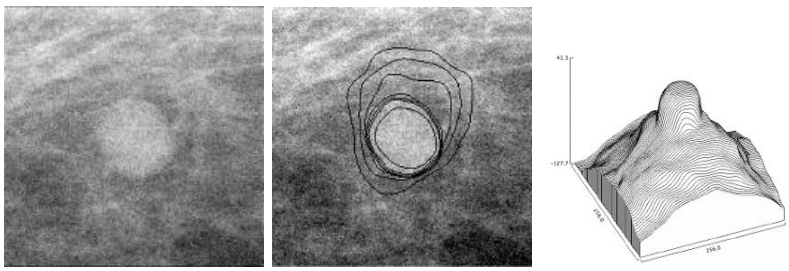

(a) (b) (c)

Figure 2. Fuzzy active contour. The original image (a) is segmented using the energy of Equation 2. The resulting ϕ (c) is sliced in order to get a set of possible contours (b).

For each contour, an energy value is computed and a membership value to the class *contour* is derived from this one. The energy value is obtained from Equation 2 by shifting the function to the level of the considered contour. This shift is done by adding a constant value to ϕ such that the zero level of the shifted function corresponds to the selected contour. To compute the energy, more strict approximations of δ and H are used. Then the candidate with the lowest energy (e_{min}) is considered to completely verify the property *is a contour*,

and thus a membership value of 1 is associated to it. The remaining contour membership values are computed using:

$$\mu(\mathcal{C}) = \max(0, 1 - c * (e_{\mathcal{C}} - e_{min})) \tag{6}$$

where c is a positive constant, $\mathcal{C}$ the considered contour and $e_{\mathcal{C}}$ its energy.

These contours are nested and thus ordered: they represent a fuzzy contour. Using a partial de-fuzzyfication process,[2] fuzzy contours from different projections are associated, leading to a marker in the volume. Re-projecting each 3D marker derived from this aggregation (using an operator as the arithmetical mean) allows the association of fuzzy contours over the projections.

4. CLASSIFICATION USING FUZZY DECISIONS TREES

In order to classify the lesion, attributes are extracted from the contours. Since the segmentation results are not crisp, and one finding is represented by several fuzzy contours retrieved from different projections, it is difficult to use classical classification tools. The fuzzy framework is suitable to deal with these constraints: it enables us to express attribute values from fuzzy contours using the extension principle,[9] to merge information from different sources (the projections) and to classify them using fuzzy decision trees. This is the main contribution of this paper.

4.1 Fuzzy attribute extraction

For every crisp contour of a fuzzy contour some common attribute values (compacity, homogeneity, gradient orientation, etc.) are computed.[10] Using the extension principle,[9] fuzzy attribute values can be calculated for the fuzzy contour from these crisp values. The extension principle is illustrated in Figure 3.

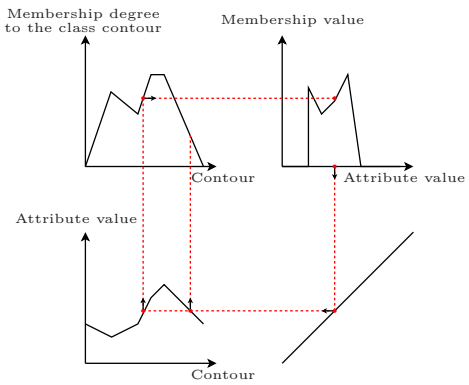

Figure 3. Extension principle: for every possible value of the attribute, the contours with this attribute value are considered, and the maximum membership degree of these contours is associated to the attribute value.

4.2 Aggregation of particles over the projections

Since a marker in space is associated to fuzzy contours in different projections, the fuzzy features of these contours need to be aggregated. The result of this aggregation is named a cumulated fuzzy attribute. This value is representative of the finding from the different projections. The classifier will be fed with this fuzzy value. This aggregation is done for each attribute in a disjunctive way using a t-conorm (fuzzy union: e.g. max) as illustrated in Figure 4.

4.3 Fuzzy decision tree

Finally, fuzzy decision trees are used to check whether the former assumptions hold. These trees not only propagate the input into every branch with a membership degree, they are also able to handle fuzzy inputs.[10] These inputs are composed of a set of fuzzy quantities (the fuzzy cumulated attributes previously computed) associated to the different attributes.

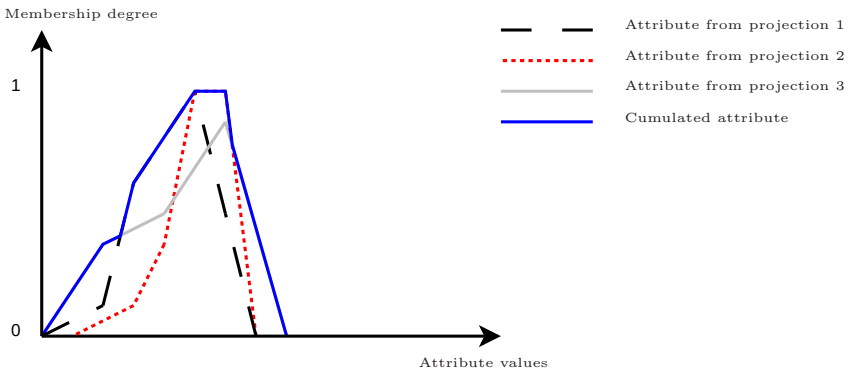

Figure 4. Computation of a cumulated (solid line) attribute from a fuzzy attribute from three projections.

4.3.1 Fuzzy tree description

Such a tree is similar to classical fuzzy decision trees where each internal node of the tree is associated to an attribute and composed of two density functions leading to two sub-trees. The density function of each sub-tree is a representative generalization of the population going in this one. In the case of spiculated a priori, the leaves are labeled as *spiculated lesion* or *not spiculated lesion* (denoted herein as A and $\overline{A}$), and in the case of circumscribed a priori as *circumscribed lesion* or *not circumscribed lesion*. Figure 5 illustrates the structure of such a tree.

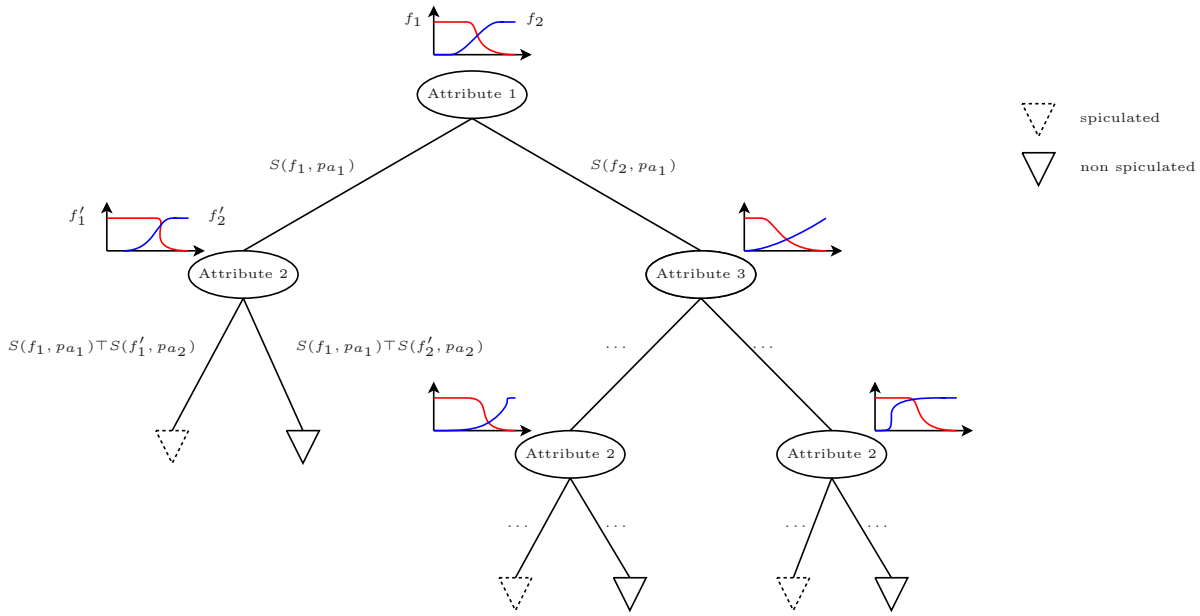

Figure 5. Tree description. Each internal node is associated to an attribute and contains two density functions corresponding to two subbranches. Each leaf is tagged either as spiculated (resp. circumscribed) or non spiculated (resp. non circumscribed).

4.3.2 Fuzzy tree usage

To classify a fuzzy particle using this tree, it is processed as follows (see Figure 5):

- the particle p moves to a node (associated to an attribute a) with a membership degree μ,

- for each density function f_i^a of this node, a similitude $S(f_i^a, p_a)$, with p_a the corresponding attribute value of p, is computed,
- the particle is then propagated into the sub-trees with the membership value:

$$\mu \top S(f_i^a, p_a) \tag{7}$$

where $\top$ is a t-norm (here the min is chosen).

In our experimentation the similitude measure between two fuzzy sets f and h was defined as:[10]

$$S(f,h) = \frac{\int_x \min(f(x), h(h))dx}{\int_x h(x)dx}$$

Thus, when a particle is passed through the whole tree, we get for each leaf a degree for the particle to arrive in this one (μ_l). To make a final decision, the results of the leaves are aggregated using a t-conorm $\perp$. This results in two degrees μ_A and $\mu_{\overline{A}}$:

$$\begin{aligned} \mu_A &= \underset{l \in \mathcal{L}}{\perp} \mu_l \\ \mu_{\overline{A}} &= \underset{l \in \overline{\mathcal{L}}}{\perp} \mu_l \end{aligned} \tag{8}$$

with $\mathcal{L}$ the set of leaves tagged as A, and $\overline{\mathcal{L}}$ the set of leaves tagged as $\overline{A}$.

In our case, two trees, which are working directly on the fuzzy attributes previously computed and aggregated, are constructed (one per assumption). For each finding in space, the aggregation of segmentations using a priori is processed in the corresponding tree. Thus each finding is processed by the two trees in parallel, resulting in four satisfaction degrees of the following properties: the finding is/is not circumscribed, and the finding is/is not spiculated.

4.3.3 Tree construction

To construct the trees, we use a recursive algorithm on each node, which relies on a training database of particles labeled as class A or class $\overline{A}$. This algorithm starts from the root and works as follows:

- choose the most discriminant attribute,
- compute density node tests for the two branches from the database,
- make every particule from the database pass through both sub-trees (using Equation 7) and iterate the process on them,
- stop when a purity criterion is reached, or when there is no more attribute (all have been used).

The purity of a leaf can be expressed as:

$$\frac{\sum_{p/class(p)=A} \mu(p)}{\sum_p \mu(p)} \geq t \quad or \quad \frac{\sum_{p/class(p)=\overline{A}} \mu(p)}{\sum_p \mu(p)} \geq t \tag{9}$$

with t the purity threshold, p the elements of the training database and $\mu(p)$ the degree they arrive in the leaf with.

Thus we mainly need a way to select the best attribute, and a procedure to compute density functions for that node. To achieve the last step, for each class a fuzzy histogram is computed: each fuzzy attribute value is normalized by the area under its curve, and weighted by the degree it enters the node with. The area of the fuzzy attribute histogram is also normalized to 1. This is equivalent to say that we impose for the histograms to

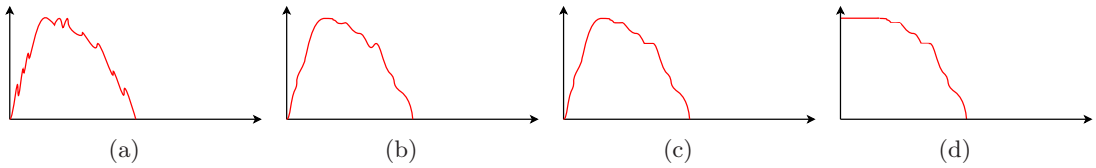

Figure 6. Histogram computation. Original histogram (a) processed with a median filter and a mean filter (b) then reconstructed (c) and finally extended (d).

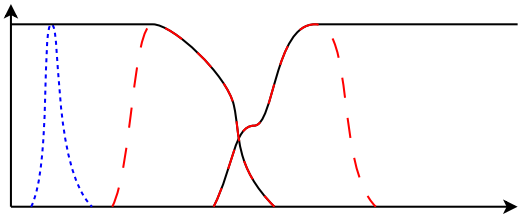

Figure 7. Test functions for a node. The two unextended histograms (dashed line) are not suitable to classify a particle (dotted line) that has a value not represented by the population used for their construction. The extended version of these histograms (solid line) does not suffer from this limitation.

contain an equal number of attribute values in order to be able to compare them. To be more robust to noise and to be able to generalize the learning data, this histogram is processed using median and mean filters, then reconstructed and its maximum is extended to the domain limit (see Figure 6) resulting in a suitable density function. The last extension step is important since it allows to make a decision for particules that have values outside the range used for learning as shown in Figure 7.

Using these density functions, it is possible to evaluate how discriminant an attribute a is according to the training database elements arriving in a given node S_k with membership values μ_{S_k} using an entropy gain measure[11] defined as:

$$Gain(S_k, a) = Entropy(S_k) - \sum_{b \in sub-branches} \frac{|C_{S_k}^{b|a}|}{|C_{S_k}^{a}|} Entropy(S_k^{b|a}) \tag{10}$$

with:

$$C_{S_k}^i = \sum_{class(x)=1 \ \wedge \ x \in supp(S_k)} \mu_{S_k}(x) \qquad C_{S_k} = \sum_i C_{S_k}^i$$
$$P_i^{S_k} = \frac{C_{S_k}^i}{C_{S_k}} \qquad Entropy(S_k) = -\sum_i P_i^{S_k} log_2 P_i^{S_k}$$

and for a given branch b, $S_k^{b|a}$ the elements of the training database valued by their membership degree when they arrive in the sub-branch b ($\mu_{S_k}(p) \top S(f_b^a, p_a)$).

Some other approaches exist like contrast measurements,[2,10] but they seems to be unsuitable for noisy/non discriminant attributes.

The leaves' labels are simply assigned according to the most representative (sum weighted with membership degrees) class of elements arriving in these ones.

5. DECISION MAKING

For each finding, we have two fuzzy particles (one per assumption) processed by two distinct fuzzy decision trees. It is then possible that the two trees do not make consistent decisions: for instance, a finding can be said to be spiculated and circumscribed at the same time.

In case of conflict between the two models, a confidence degree is computed on the outputs (A and $\overline{A}$) of each tree:[10]

$$D_A = \frac{|\mu_A - \mu_{\overline{A}}|}{\mu_A + \mu_{\overline{A}}}$$

Such a degree represents how much a tree is confident in its decision: if μ_A and $\mu_{\overline{A}}$ are very close to each other, it is most likely that the tree is unable to make a decision for the considered particle. Using these confidence degrees (D_{cir} and D_{sp}), the outputs (membership values μ_{sp}, $\mu_{\overline{sp}}$, μ_{cir} and $\mu_{\overline{cir}}$ to the classes *spiculated*, *not spiculated*, *circumscribed* and *not circumscribed*) of the trees can be weighted in order to get the most suitable decision:

$$\begin{cases} \text{the mass is circumscribed if } \max(D_{cir}\mu_{cir}, D_{sp}\mu_{\overline{sp}}) > \max(D_{cir}\mu_{\overline{cir}}, D_{sp}\mu_{sp}) \\ \text{the mass is spiculated otherwise} \end{cases}$$

6. RESULTS

As previously said, only the segmentation/classification parts of the approach was evaluated. After describing the database used, we discuss results obtained for each part of the method.

6.1 Database

The DBT data sets used in this study have been acquired with a GE DBT investigational device at the Massachusetts General Hospital (MGH), Boston, MA, USA. For each breast, 15 projected views have been acquired over an angular range of 30 degrees. To guarantee an overall patient dose that is not superior to the dose delivered in standard mammography, the dose per projection image is reduced to approximately 10 % of the dose delivered to the patient during a mammography examination. All acquisitions have been performed in a medio-lateral oblique (MLO) view. No clinical ground truth was available for the image data (neither radiologists reports nor histology results). We have therefore performed a screening of selected cases with several medical imaging experts. The screening of the clinical cases was first performed on slices reconstructed with Simultaneous Algebraic Reconstruction Technique[12] (SART). We have then identified the corresponding ROIs in the tomographic projection images. The set of 23 breast masses have been identified from 9 different DBT data sets. The database consists of 16 spiculated breast masses and 7 circumscribed breast masses. Because of the reduced dose in the projected views, some of the masses are very difficult to distinguish in these images. For the same reason, the database presents a considerable challenge for testing our CAD framework.

Due to the size of the data base, the leave-one-out method was most suitable to validate the approach: each element of the data base is classified with trees trained with the remaining elements.

6.2 Contour extraction

Some segmentation results for both active contours models are illustrated in Figure 8 on a circumscribed mass and a spiculated one. In the case of the circumscribed mass, even if contours obtained for the spiculated assumption are less regular, a large number of contours fits the actual contour well. In the case of the spiculated lesion, the contour given by the expert is more subjective. This justifies the extraction of several contours, and thus the usage of the fuzzy sets framework. The contours obtained for the two assumptions are rather different: the circumscribed model is unable to get the spicules whereas the other model succeeds.

6.3 Feature extraction

Examples for computation of cumulated attributes applied on a clinical ROI containing a circumscribed breast mass and for a clinical ROI containing a spiculated breast mass are illustrated in Figure 9. For the circumscribed mass a high compacity (around 0.8) has been measured for most candidate contours in the projected views. This information is translated to the cumulated fuzzy attribute where values around 0.8 for the compacity of the particle are indicated to be most representative for the particle. For the spicualted mass in Figure 8(d) lower

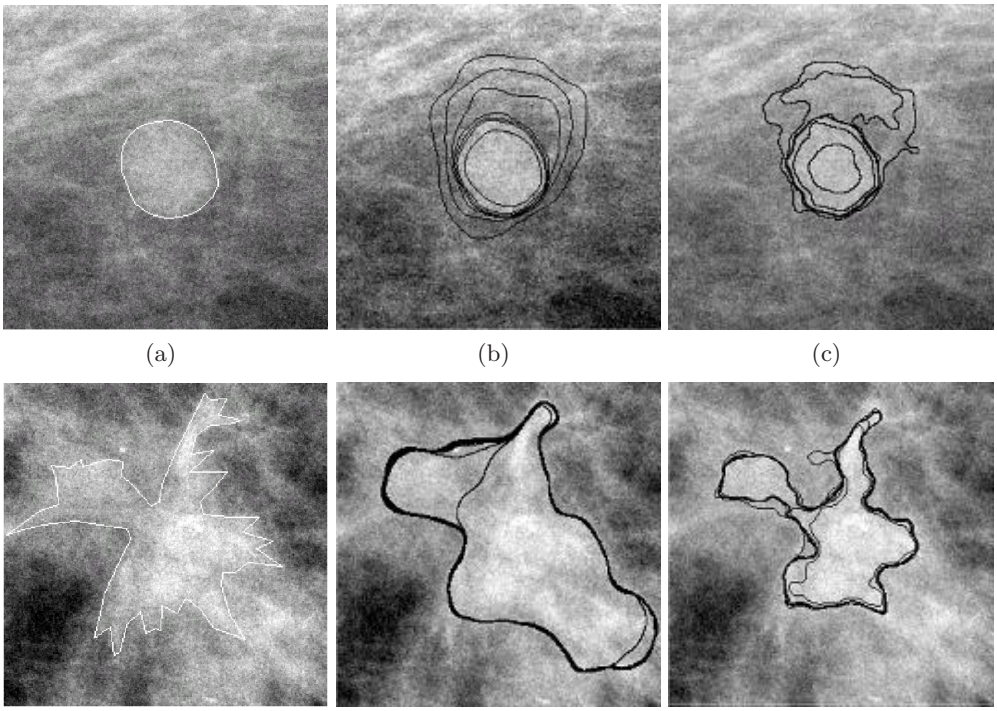

Figure 8. Segmentation results: a circumscribed mass segmented by an expert (a), using circumscribed (b), and spiculated (c) a priori, and a spiculated mass segmented by an expert (d), using circumscribed (e) and spiculated (f) a priori.

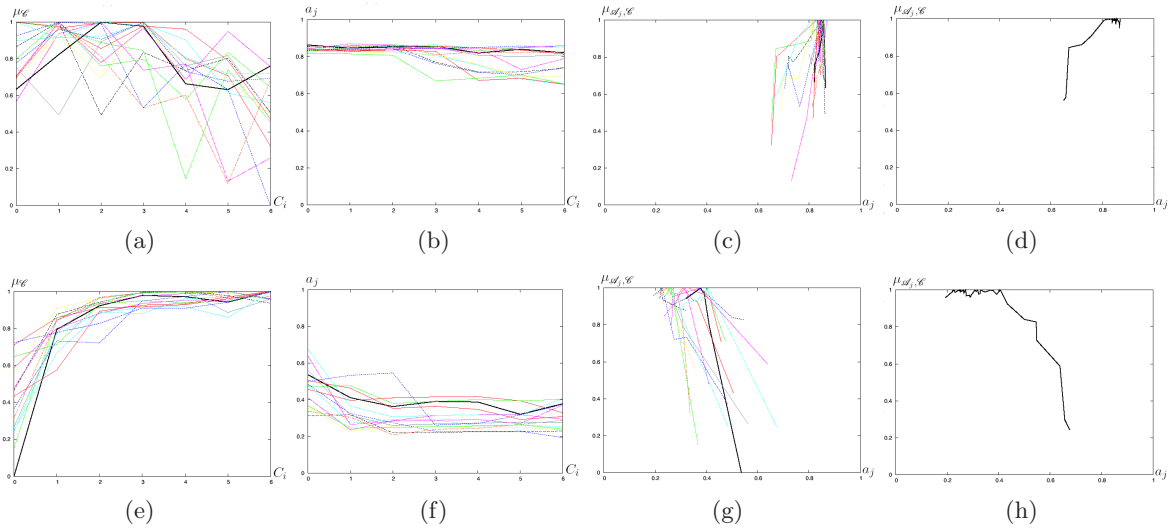

Figure 9. Aggregation of fuzzy attributes extracted from ROI containing a circumscribed (resp. spiculated) lesion presented in Figure 8(a) (resp. Figure 8(d)): (a) (resp. (e)) corresponding membership functions to the class contour, (b) (resp. (f)) attribute values for the set of candidate contours for the attribute compacity, (c) (resp. (g)) superposition of the membership funtions of the fuzzy attribute and (d) (resp. (h)) the resulting membership function for the cumulated fuzzy attribute. In (a-c) (resp. (e-g)) the different curves represent values for different projected views. The solid black line corresponds to the 0-degree projection depicted in Figure 8(a) (resp. Figure 8(d)) and Figure 8(b) (resp. Figure 8(e)).

compacity values have been computed. Furthermore, the variance of the different projected views is higher than

in the one obtained for the circumscribed case. This leads to a higher ambiguity in the cumulated fuzzy attribute function. Values between 0.2 and 0.45 seem to be equally representative of the particle. The obtained cumulated fuzzy attributes express that a high compacity is characteristic for the circumscribed breast mass in Figure 8(a) while a low compacity is characteristic for the spiculated breast mass in Figure 8(d). This corresponds well to the intuitive interpretation of the respective examples.

6.4 Classification

Figure 10(a) provides error rates for the classification part: in 57% of the cases both trees give a good classification, in 39% they disagree, and in 4% they are both wrong. Using confidence degrees some conflicting cases can be resolved, resulting in a total classification error rate equal to 9% (see Figure 10(b)). This clearly shows the gain of using two different assumptions to characterize the lesions: only one segmentation model would not be sufficient (the circumscribed and spiculated models are wrong in respectively 13% and 30% of the cases).

Along the iterations of the leave-one-out process, the tree corresponding to the circumscribed assumption was mostly constructed using three attributes: the compacity, the mean gradient value on the contour and the mean gradient orientation compared to the center of the mass on the contour. In addition, the second tree corresponding the spiculated hypothesis was relying on the mean of the gradient within the ROI.

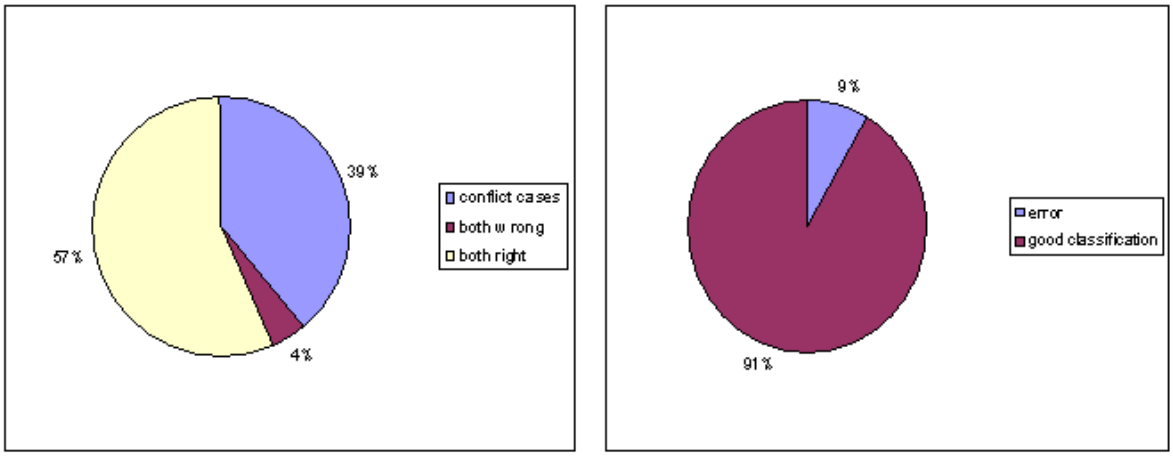

(a) (b)

Figure 10. Classification error rates. Unmerged results from both classifiers (a), and final classification error rate (b).

7. CONCLUSION

We have proposed a global scheme for mass detection/classification based on fuzzy sets. This approach relies on two key ideas. First, fuzzy sets are used to handle uncertainty until all the information from different projections is available (aggregation of fuzzy attributes). Second, two hypotheses are made in order to be validated or invalidated during similar processes (only the a priori information introduced in the segmentation process changes). This last step can lead to conflict in the decision since the two processes associated to the former hypotheses are independent. For that reason we introduced a way to resolve such cases.

This segmentation/classification approach has been evaluated on a data base composed of 23 real masses. Even if statistics about the error rates obtained with such a small database are not completely reliable, the results tend to validate the approach to make two different assumptions and to try to validate/invalidate them.

REFERENCES

[1] Cheng, H. D., Shi, X. J., Min, R., Hu, L. M., Cai, X. P., and Du, H. N., "Approaches for automated detection and classification of masses in mammograms," *Pattern Recogn.* 39(4), 646–668, (2006).

[2] Peters, G., [Computer-aided Detection for Digital Breast Tomosynthesis], PhD thesis, Ecole Nationale Supérieure des Télécommunications, (2007).
[3] Peters, G., Muller, S., Bernard, S., and Bloch, I. [Soft Computing and Image Processing: Recent Advances], Springer-Verlag, ch. Wavelets and Fuzzy Contours in 3D-CAD for Digital Breast Tomosynthesis, 296–323, (2006).
[4] Osher, S. and Sethian, J., "Fronts propagating with curvature-dependent speed: Algorithms based on Hamilton-Jacobi formulations," *Journ. Computational Physics* 79, 12–49, (1988).
[5] Osher, S. J. and Fedkiw, R., [Level Set Methods and Dynamic Implicit Surfaces], Springer, (2002).
[6] Peters, G., Muller, S., Grosjean, B., Bernard, S., and Bloch, I., "A hybrid active contour model for mass detection in digital breast tomosynthesis," in *Medical Imaging 2007: Computer-Aided Diagnosis*, *Proceedings of the Society of Photo-Optical Instrumentation Engineers (SPIE) Conference* 6514-1V, 1–11, (2007).
[7] Chan, T. and Vese, L., "Active contours without edges," *IEEE Trans. Image Processing* 10(2), 266–277, (2001).
[8] Gout, C., Guyader, C. L., and Vese, L., "Segmentation under geometrical conditions using geodesic active contours and interpolation using level set methods," *Numerical Algorithms* 39, 155–173(19), (2005).
[9] Zadeh, L. A., "The concept of a linguistic variable and its application to approximate reasoning-III," *Information Sciences* 9(1), 43–80, (1975).
[10] Bothorel, S., [Analyse d'images par arbre de décision flou], PhD thesis, Université Paris VI, (1996).
[11] Lee, K.-M., Lee, K.-M., Lee, J.-H., and Lee-Kwang, H., "A fuzzy decision tree induction method for fuzzy data," *Fuzzy Systems Conference Proceedings* 1, 16–21, (1999).
[12] Andersen, A. H. and Kak, A. C., "Simultaneous algebraic reconstruction technique (SART): A superior implementation of the art algorithm," *Ultrasonic Imaging* 6(1), 81–94, (1984).